TU Delft

Delft University of Technology

Coherent Raman imaging thermometry with in-situ referencing of the impulsive excitation efficiency

Mazza, Francesco; Castellanos, Leonardo; Kliukin, Dmitrii; Bohlin, Alexis

DOI
10.1016/j.proci.2020.06.360

Publication date
2020

Document Version
Accepted author manuscript

Published in
Proceedings of the Combustion Institute

Citation (APA)
Mazza, F., Castellanos, L., Kliukin, D., & Bohlin, A. (2020). Coherent Raman imaging thermometry with in-situ referencing of the impulsive excitation efficiency. *Proceedings of the Combustion Institute*, *38*(1), 1895-1904. https://doi.org/10.1016/j.proci.2020.06.360

Important note
To cite this publication, please use the final published version (if applicable).
Please check the document version above.

Copyright
Other than for strictly personal use, it is not permitted to download, forward or distribute the text or part of it, without the consent of the author(s) and/or copyright holder(s), unless the work is under an open content license such as Creative Commons.

Takedown policy
Please contact us and provide details if you believe this document breaches copyrights.
We will remove access to the work immediately and investigate your claim.

This work is downloaded from Delft University of Technology.
For technical reasons the number of authors shown on this cover page is limited to a maximum of 10.

Coherent Raman imaging thermometry with *in-situ* referencing of the impulsive excitation efficiency

Francesco Mazza, Leonardo Castellanos, Dmitrii Kliukin, and Alexis Bohlin*

Faculty of Aerospace Engineering, Delft University of Technology, Kluyverweg 1, 2629 HS Delft, The Netherlands

Alexis Bohlin* (Corresponding Author*), g.a.bohlin@tudelft.nl, (tel) +31 15 27 89231

Abstract

Simultaneous detection of resonant and non-resonant femtosecond/picosecond coherent anti-Stokes Ra- man spectroscopy (CARS) signals has been developed as a viable technique to provide *in-situ* referencing of the impulsive excitation efficiency for temperature assessments in flames. In the framework of CARS ther- mometry, the occurrence of both a resonant and a non-resonant contribution to the third-order susceptibility is well known. While the resonant part conceives the useful spectral information for deriving temperature and species concentrations in the probed volume, the non-resonant part is often disregarded. It nonetheless serves the CARS technique as an essential reference to map the finite bandwidth of the laser excitation fields and the transmission characteristics of the signal along the detection path. Hence, the standard protocols for CARS flame measurements include the time-averaged recording of the non-resonant signal, to be performed sequentially to the experiment. In the present work we present the successful single-shot recordings of both the resonant and non-resonant

CARS signals, split on the same detector frame, realizing the *in-situ* refer- encing of the impulsive excitation efficiency. We demonstrate the use of this technique on one-dimensional CARS imaging spectra, acquired across the flame front of a laminar premixed methane/air flame. The effect of pulse dispersion on the laser excitation fields, while propagating in the participating medium, is proved to result, if not accounted for, in an ∼1.3% systematic bias of the CARS-evaluated temperature in the oxidation region of the flame.

Keywords: gas-phase thermometry; CARS; coherent imaging; non-linear susceptibility; combustion diagnostics

1. Introduction

Laser diagnostics is an important tool in the effort to develop clean combustion technology, which is on the agenda for the propulsion and power industry in-line with the current energy transition. These optical techniques have the ability to realize non-intrusive measurements *in-situ* and to provide scalar information (e.g. temperature and species) with excellent spatial and temporal resolution. Laser diagnostics has been used successfully employed over the years in multiple energy and combustion science applications where high-fidelity data are needed [1,2], e.g. by providing direct observations and validating results from predictive combustion engineering models.

Coherent anti-Stokes Raman spectroscopy (CARS) is a versatile technique for assessing temperature and species concentration in flames. It is unparalleled in the level of accuracy and precision it can provide, and the strong “laser-like” signal, which can be detected remotely from where it is generated, makes it well-suited for the application in

extremely harsh and luminous environments, such as combustion flows [3,4,5]. The conventional setup for CARS spectroscopy is based on nanosecond pulses; however, many variants exist, in which the inaccuracy and precision are technique-specific and need to be quantified respective to the measurement environment (nanosecond CARS thermometry has an approximate inaccuracy of ~2-3%, and a single-shot imprecision of ~4-5% [6,7]). In air-fed flames, the temperature sensitivity arises from the relative strength of the N_2 spectral lines. The spectrum uncovers the Boltzmann distribution (in principle) over the entire manifold of molecular rotational-vibrational states in the thermal ensemble. The retrieval of the quantitative temperature information from a CARS experiment is enabled by the combination of unobstructed detection of the spectrum and adequate spectroscopic modelling: the recorded data is evaluated using a goodness of fit routine [8].

The uncertainty in CARS-evaluated temperature is related to critical parameters, leading to either systematic (inaccuracy) or stochastic (imprecision) deviation from the true temperature. Much effort has been spent in quantifying the overall accuracy of the technique and limiting the impact of uncertainties originating from e.g. pressure broadening (Raman linewidths) [9], from the vibrational-rotational matrix-elements (Herman-Wallis factor) [10], and from the mode-amplitude and phase-mode fluctuations on the broadband laser emission profiles [11,12]. The influence of uncertainty originating from the non-resonant susceptibility has also been investigated [13], although most of the effort in dealing with this parameter in CARS thermometry has been spent on the spectral fitting routine. This is partly because the total non-resonant susceptibility depends not only on the active molecule (e.g. N_2), but also on contributions from the background species [14,15]. A perfectly validated theoretical value of the non-resonant susceptibility, to be included in the spectral fitting routine, would require the complete experimental recovery of chemical composition of the sample. The relative strength of the resonant and non-resonant CARS susceptibility is not only relevant for thermometry, but has been commonly employed for extracting species concentration as well. This technique is particularly interesting to detect water vapour [16,17], which is a recognized challenge for CARS diagnostics because the relatively low Raman cross-section of the H_2O molecule [18].

The implementation of time-resolved CARS allows for reducing the impact of many of the aforementioned sources of uncertainty [19,20,21]. With time-resolved CARS probing we refer not only to the freezing of the energy-

containing scale in the combustion flow (achieved on a microsecond timescale), but also to the fact that the probing time is well within the characteristic molecular response time (dephasing). This temporal window for probing combustion-relevant species is usually on a picosecond timescale, the relatively long dephasing time of hydrogen being an exception [22]. On this short timescale the impact on the CARS spectrum of the Raman linewidths is small. Also the mode-amplitude and phase-mode fluctuations, affecting the emission profile of the broadband laser, are significantly reduced by using a near transform-limited femtosecond laser pulse, as compared to the output from a nanosecond pumped dye-laser. In addition, through a time-resolved CARS technique, the suppression of the non-resonant four-wave mixing signal is achieved by simply delaying the probe pulse relative the pump and Stokes pulses [23,24]. Recent investigations aimed at the benchmarking of time-resolved CARS thermometry [25,26,27] have shown a considerably reduced relative standard deviation with respect to nanosecond CARS thermometry, reaching the unprecedented single-shot precision of ~1% in room air and ~1-3% in flames. When operating in flames, it is nonetheless difficult to make perfect statements about the statistical uncertainty inherent to the CARS technique. Indeed, the measured temperature might be effected by fluctuations in the experimental boundary conditions e.g. originating from factors related to the flow controllers and vibrations of the platform. In order to determine the overall accuracy of CARS-evaluated temperature, a similarity test with other experimental techniques and comparison to numerical simulations is thus important [28].

In the present work, we develop a technique aimed at minimizing the influence on CARS thermometric uncertainty resulting from the effective bandwidth of the laser excitation fields. In turbulent flames and flows, the temperature and species gradients (and, accordingly, the number density of the gas mixture) changes constantly with respect to the alignment of the laser excitation fields [29]. Therefore, shot-to-shot fluctuations may occur *in-situ*, affecting the delivery of a uniform bandwidth and the phase-matching condition, necessary to coherently drive the temperature sensitive CARS transitions. However, even in more still, stationary measurement conditions (e.g. in a laminar flame), which allow statistics to be obtained from signal averaging, the CARS spectrum depends on the effective bandwidth of the laser excitation fields, as imposed by the measurement conditions. In this framework, the simultaneous referencing of the excitation efficiency has been developed to improve the CARS thermometric measurements obtained on the principle of a single-laser-shot [16,30]. Here, we use the non-resonant CARS

susceptibility, measured *in-situ*, to extract information on the effective impulsive efficiency, mapped directly by the spectrum of the non-resonant four-wave mixing signal. Concurrent resonant and non-resonant CARS signals are generated in the flame, and simultaneous detection of both the signals is achieved through a novel polarisation sensitive wide-field coherent imaging spectrometer. We demonstrate the use of this spectrometer on spatially-correlated data, generated with single-shot femtosecond/picosecond 1D-CARS. We analyze the potential of the simultaneous, *in-situ* referencing in reducing the thermometric uncertainty, as compared to a standard protocol, where the spectral referencing is provided by a recording sequential to the experiment.

2. Theoretical Considerations

In dual-broadband pure-rotational CARS [31,32], two-photon constructive pairs, available across the bandwidth of the laser excitation fields, coherently drive specific Raman shifts in the spectral range of ~0-500 cm^{-1}. This corresponds to N_2 pure-rotational S-branch transitions from quantum numbers J's = 0 - 60, characterised by $\Delta\varepsilon_{J,\,J+2} = 4B\,(J+3/2)$, with $4B$ ~8 cm^{-1} for N_2. In femtosecond/picosecond CARS [26,33,34,35,36,37,38,39], the excitation efficiency across a specific Raman-active window is dictated by the finite bandwidth of the transform-limited fs-duration driving pulse. When considering pure-rotational CARS transitions ($\Delta v=0$, $\Delta J=+/-2$, $\Delta M_J=0$), the laser excitation of the molecules results in a non-adiabatic interaction (here termed "impulsive") if the laser pulse duration is about one tenth of the molecular rotational period [40]. The impulsive excitation of N_2, for which the rotational periods are in the order of ~500 fs, would require a ~50 fs duration laser pulse. The high excitation-efficiency provided by the impulsive drive of the rotational Raman transitions, is a prerequisite for generating non-resonant four-wave mixing signals at appreciable signal levels, for the instantaneous detection in gaseous high-temperature gaseous environments. In general, the strength of the CARS signal scales to the number density squared, and the number density is inversely proportional to the temperature in the sample.

The polarization dependence on the resonant- and non-resonant CARS signals [41] is described with angles $\tan \beta = -\sin \phi / 2 \cos \phi$ for the resonant CARS signal and $\tan \delta = \sin \phi / 3 \cos \phi$ for the non-resonant CARS signal, determined as a function of the incident relative angle, ϕ, between the probe beam and the pump/Stokes beams,

respectively. The probe angle of 67.5° relative the vertically polarized pump/Stokes beam results in orthogonally polarized resonant and non-resonant CARS signals.

3. Experimental

The experimental setup was implemented according to the two-beam femtosecond/picosecond phase-matching scheme for 1D-CARS imaging [42], here achieved with a single regenerative amplifier laser system [43]. The laser pulses originate as the ~35 fs output of a high-power femtosecond regenerative amplifier, with a pulse energy of ~7.5 mJ provided at a 1 kHz repetition-rate (Astrella, Coherent). A narrowband ~7 ps-duration full-width-at-half-maximum (FWHM) probe pulse centered at ~402 nm, is efficiently produced by means of second-harmonic bandwidth compression [44,45] (Light Conversion), and converted from a ~65% portion of the fs laser output. This results in the ps probe pulse being both repetition-wise synchronized with the fs pump/Stokes pulse and automatically phase-locked at the CARS measurement, with an arbitrary arrival time. The near transform-limited fs pump/Stokes pulse is produced by an external compressor operating on a ~35% portion split of the uncompressed output from the amplifier. This design allows for flexible compensation (pre-chirping) of dispersion terms possibly arising along the optical path, thus providing impulsive excitation at the CARS measurement. The alignment of the laser beams and the polarization sensitive detection of the single-shot femtosecond/picosecond 1D-CARS signals is depicted in Fig. 1.

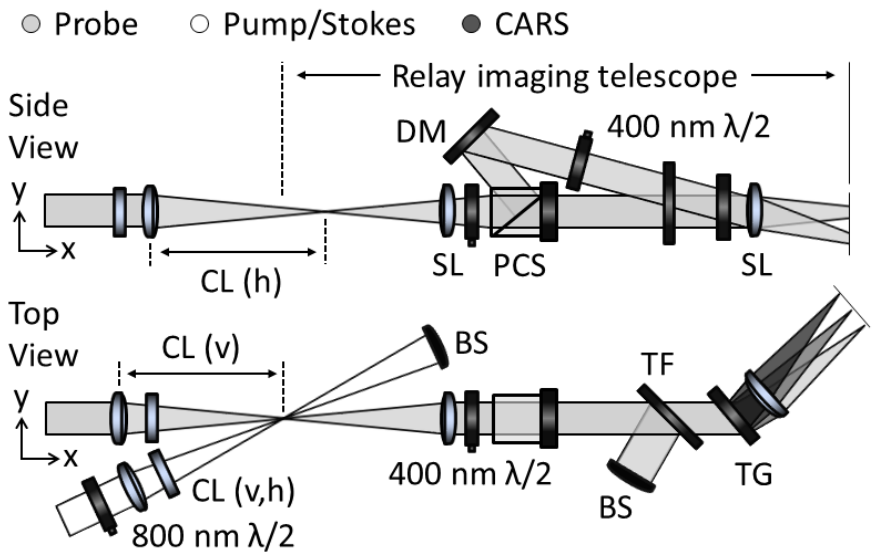

Fig. 1. The polarization-sensitive wide-field coherent imaging spectrometer used for spatially divided detection of reso- nant - and non-resonant hybrid femtosecond/picosecond one-dimensional (1D) coherent anti-Stokes Raman spectroscopy (CARS) signals. The indexes v (vertically) and h (horizontally) express the alignment symmetry axis of the cylindrical lenses cylindrical lenses (CL). Two separate detection channels for P- and S-polarized light, with orientation determined with respect to the transmission grating (TG), are relay-imaged with ~1:1 magnification from the signal generation plane to the position of the detector. DM-dichroic mirror, PCS-polarization cube splitter, BS-beam stop, TF-tunable filter, and SL-spherical lens.

The ~2.3 mJ impulsive excitation beam (femtosecond laser pulse) and the ~0.4 mJ probe beam (picosecond laser pulse) are intersected in a crossed-plane geometry forming a one-dimensional spatial coordinate. The two beams are synchronized by an optical delay-line made of a high-finesse translation stage, ensuring sub-picosecond temporal resolution. The levelling and relative polarization of the laser beams are controlled with turning periscopes and a half-wave plate (Eksma optics) mounted in the pump/Stokes beam path; the shaping of the laser beams is performed with low-dispersion sheet-forming optics. The irradiance (~1 J/cm^2) of the probe beam is significantly enhanced at the measurement location by means of astigmatic convergence [46], here realized by two cylindrical lenses with focal lengths f=300 mm (v,h) -the indexes v (vertically) and h (horizontally) express the alignment symmetry axis, respectively. In efforts to match the phase-matching condition homogeneously across the line-image, a combination of focal lengths f=500 mm (v) and f=1000 mm (h) is employed in the pump/Stokes beam path. However, the phase-matching condition is relaxed for driving pure-rotational N_2 CARS transitions with the

current beam conditioning. The excitation beam is dumped before the first collection lens in the wide-field, one-to-one plane, coherent imaging spectrometer, while the probe beam is separated from the pure-rotational CARS signal through the angle-tuning of a spectral bandpass filter (Semrock). The resonant and non-resonant CARS signals are separated in two polarization-dependent detection channels, composed by two 400 nm half-wave plates and a polarization cube splitter (Eksma optics). Both channels are directed through a transmission grating (3040 lines/mm, Ibsen Photonics) and relay-imaged onto the same detector plane (Zyla 4.2, Andor). The first half-wave plate rotates the cross-polarized resonant and non-resonant CARS signals to fit the orthogonal S- and P-polarization transmission axes of the analyser. The second half-wave plate is mounted after the analyser to turn the polarization of the non-resonant CARS signal from P- to S-polarization and achieve the maximum grating transmission efficiency of >90% at 400 nm.

The measurement was performed across the flame-front of a premixed laminar methane/air flame (Φ=0.95), provided on a Bunsen burner. The fuel (methane) and oxidizer (air) are delivered from separate containers, and variable area flow meters (rotameters) provide independent control over each of the flows. Upon exiting the rotameters the flow lines are connected to a junction, after which the gases are mixed and the mixture is provided with a total bulk flow velocity of ~1 m/s. The combustible mixture is then channeled through a seamless stainless burner pipe, designed with a length to diameter ratio (~1:100) more than sufficient to dampen coherent flow structures and provide a laminar flow at the exit (Reynolds number < 2000). The 10 mm inner diameter nozzle is shaped conical to minimize heat losses at the burner rim. The probe volume was positioned in proximity of the chemical reaction layer, and oriented so as to provide measurements along a line orthogonal to the flame front.

The crossing angle (θ) of the pump/Stokes and probe beams was measured to 3°, providing a probe volume of ~0.03 mm (width) x ~0.6 mm (length) x ~1.3 mm (height), estimated from the assumption of a near diffraction limited beam waist (e_0) of 30 µm FWHM (width), yielding an interaction length of $e_0/\sin(\theta)$ = 0.6 mm. The total field-of-view (FOV) was measured to ~1.3 mm (height) and the image quality was retrieved with a ~40 µm line-spread function (LSF). These parameters were measured as the translation (FOV) and steepness (LSF) of an edge response in the signal, resulting from inserting a razor blade at the plane of the two-beam crossing. An ~3 ps relative temporal delay between the excitation beam and the probe beam was employed in the experiment to generate the

resonant and non-resonant CARS signals simultaneously. The “time equal zero” and the probe pulse duration were calibrated by performing a probe-delay measurement scan in argon, a monoatomic gas with no rotational degree of freedom. Consequently, the only signal component is the instantaneous four-wave mixing signal, which maps the temporal profile of the ps probe beam, synchronized with the fs pump/Stokes beam. The time-averaged argon spectrum also quantifies the constructive two-photon pairs available for the excitation of a specific Raman shift and is thus employed for spectral referencing in standard protocols.

A sample of 900 single-shot, resonant and non-resonant CARS spectra was recorded simultaneously in the flame and analyzed to assess the thermometric accuracy and precision. The procedure was compared to a standard protocol, where the single-shot resonant CARS spectra are instead referenced by the time-averaged spectrum recorded from argon sequentially to the experiment.

4. Results and Discussion

Figure 2 shows the simultaneous, single-shot detection of resonant and non-resonant 1D-CARS signals, generated across the flame-front of a premixed laminar methane/air flame, and acquired on two distinct portion of the same detector frame. The labels “Channel 1” and “Channel 2” identify the portion of the detector where the resonant and non-resonant CARS signals are relayed, respectively.

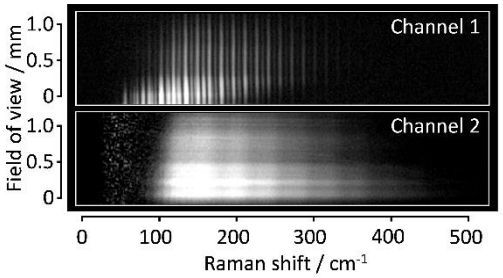

Fig. 2. Single-shot detection of concurrent resonant and non-resonant pure-rotational femtosecond/picosecond 1D-CARS signals acquired *in-situ* across the flame-front of a laminar premixed methane/air flame (Φ=0.95). The two CARS signal components are generated with a relative probe-pulse delay of ~3 ps. The label “Channel 1” indicates portion of the detector frame employed for the acquisition of the resonant CARS signal, which is dominated by the characteristic spectral signature of N_2. “Channel 2” indicates the detection channel for the broadband non-resonant CARS signal (due to four-wave-mixing), which is scattered from all the species present probed volume.

As it can be seen in Fig. 2, the resonant CARS signal is dominated by the spectral lines of the nitrogen molecules, spanning Raman shifts from ~60 cm^{-1} to 300 cm^{-1}, which result from the high-rotational energy levels being populated by the elevated temperature in the flame. The non-resonant CARS signal is instead continuous in nature, resulting from the four-wave-mixing from all the molecular species present in the sample. The highest signal intensity is detected in both channels around 180 cm^{-1}, while at frequencies lower than ~150 cm^{-1} the signals are attenuated by the angle-tuning of a spectral band-pass filter, to avoid spurious stray-light and residual probe beam reaching the detector. It is nonetheless possible to observe a speckle pattern in the spectral region spanning from ~50 cm^{-1} to ~100 cm^{-1} in the second channel, which could not be effectively suppressed by background subtraction due to its dynamic character.

Figure 3 shows a single-shot resonant spectrum acquired in the first detection channel, which is referenced by the non-resonant spectrum measured *in-situ* and detected simultaneously in the second channel.

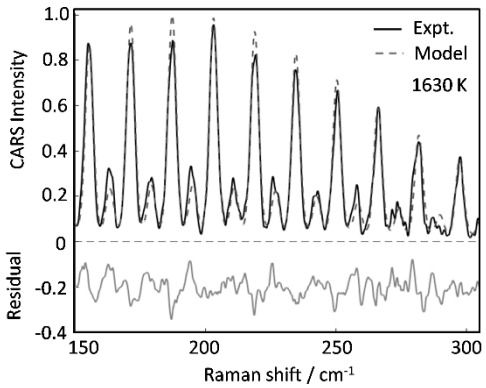

Fig. 3. Single-shot, femtosecond/picosecond resonant CARS spectrum, generated as short pump-probe pulse delay (~3ps) and acquired at ~450 μm from the flame-front of a premixed methane/air flame (Φ=0.95). The resonant spectrum, acquired in first detection channel, was back-ground subtracted and referenced to the non-resonant CARS spectrum acquired simultaneously in the second detection channel. In order to determine the corresponding temperature, the resulting spectrum was compared to a library of synthetic spectra, computed by means of a time-resolved CARS code. The resulting temperature in the measurement location was thus assessed in 1630 K. The performance of the spectral fitting can be evaluated by the residuals of the theoretical and experimental spectra, which are presented in the figure, with an offset of -0.2 for clarity purposes.

The spectral resolution of the resonant CARS signal is dictated by the linewidth of the probe beam, measured as 2.1 cm^{-1} (FWHM), as well as by the instrumental broadening resulting from the wide-field coherent imaging

spectrometer. In addition, the stray light covering the leftmost portion of the detector currently limits the spectral range available. This is nevertheless considered to have an insignificant impact on the N_2 thermometry, since, in correspondence of the elevated temperature in the product gases of the flame, the energy levels above 160 cm^{-1} are the most populated. The resonant CARS signal strength at room temperature is several order of magnitude stronger than the flame temperature signal, the signal to background ratio (SNB) rapidly degrades as a function of temperature. The estimation of the temperature from the experimental CARS spectra was performed through of a non-linear least-square contour fitting routine, comparing the acquired resonant spectrum to a library of pre-calculated theoretical spectra, for different temperature conditions. These synthetic Raman spectra were computed by means of a time-domain CARS model, similar to previously-reported ones [34,26]. The broadening of the spectral linewidths due to the imaging apparatus was accounted for by convolving the synthetic spectra with a Voigt instrument-response-function with a 1.6 cm^{-1} wide Gaussian component (FWHM) and a 0.5 cm^{-1} wide Lorentzian component (FWHM). The acquired resonant spectra were background-subtracted introducing an area-averaged factor, thus accounting for possible shot-to-shot fluctuation in the magnitude of the background. Subsequently, the spectral referencing of the impulsive excitation efficiency was performed by dividing the resonant spectrum with the non-resonant spectrum (NR) obtained through two independent methods: 1. non-resonant spectrum acquired in room-temperature argon (*ex-situ*) and 2. non-resonant spectrum acquired in the flame (*in-situ*).

In Fig. 4, the comparison of the non-resonant CARS signal provided by the two techniques is presented. The measurements were performed with spatially and temporally overlapped probe and pump/Stokes fields, at a ~3ps relative delay, for concurrent generation of the non-resonant CARS signal.

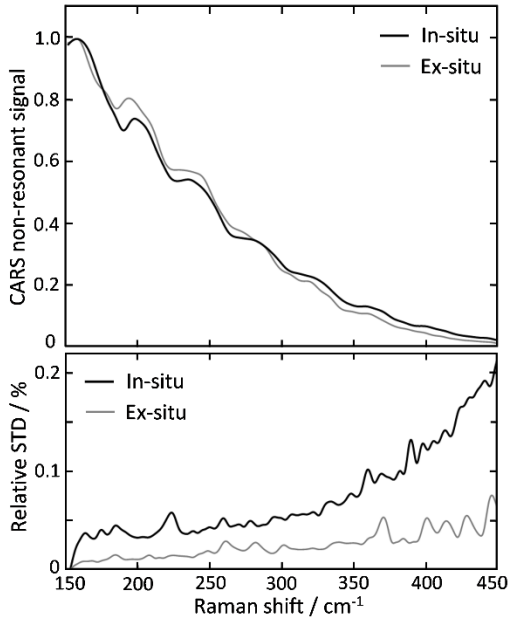

Fig. 4. (Top) Comparison of the average non-resonant spectra acquired in room-temperature argon (*ex-situ*) and at ~455 μm from the flame-front in a laminar, premixed methane/air flame (Φ=0.95). (Bottom) The relative standard deviation as obtained from the 900 instantaneous recordings.

The signal quality from each the single-shot recordings is sufficient to perform the spectral referencing: the signal counts of the single-shot spectra for the most critical condition (i.e. non-resonant signal from the flame) was ~700 counts above the baseline on the detector. The non-resonant spectra show a clear decay for increasing values of the Raman shift: in this respect, the non-resonant signal provides an effective mapping of the laser bandwidth available for the excitation of the Raman-active molecules in the ensemble. If this pronounced slope were not taken into account in the spectral fitting routine (by spectral referencing), its effect would resemble a strong *J*-dependence similar to any other critical uncertainty factor, and result in a systematic bias (inaccuracy) in the CARS evaluated temperature. The comparison of the non-resonant spectra acquired *ex-situ* and *in-situ* clearly shows that the effective bandwidth available for the excitation of the temperature-sensitive Raman transitions in the combustion products is broader than the one mapped by the non-resonant spectrum acquired in room-temperature argon. This is explained by the strong dependence of the refractive index of the participating medium (i.e. the gaseous mixture in the probe volume) on its temperature. Indeed, the group-velocity dispersion (GVD) of the fs pump/Stokes pulse induces a temporal broadening of the pulse itself as it propagates through the medium, resulting in a reduction of the effective

bandwidth [47]. As the GVD for most gases at atmospheric pressure scales linearly with the density, the high temperature of the product gases in the flame determines a significant reduction of the GVD of the pump/Stokes pulse and the increase in the effective bandwidth shown in Fig. 4.

Furthermore, if a time-average NR spectrum, acquired *ex-situ*, is employed for the spectral referencing, possible variations in the excitation bandwidth available shot-to-shot would be neglected. This behavior is expected e.g. in turbulent flames, where the temperature field, as well as the chemical composition of the gas mixture in the probe volume, are highly dynamic in nature. Seemingly, this shot-to-shot variability in the slope of the NR spectra measured the flame (*in-situ*) is neglected in the *ex-situ* measurement of the NR spectrum: this would lead to a stochastic uncertainty in the measurement. The bottom panel in Fig.4 shows the relative standard deviation (RSTD) of the NR spectra acquired *in-situ* and *ex-situ*, as a function of the Raman shift: the trend of these curves thus represents the *J*-dependence of the shot-to-shot fluctuations in the NR spectrum, i.e. in the impulsive excitation efficiency. The RSTD of the *in-situ* NR spectrum is one order of magnitude higher across the whole spectral range compared to the *ex-situ* one: this is due to the reduced SNB available in the *in-situ* measurement, as compared to the *ex-situ*, because of the decreased number density of the participating medium at high temperature. The difference in the RSTD values is more significant at the high-rotational energy levels populated at elevated temperatures: the variance of the available effective bandwidth in the fs pulse is shown to be higher in the *in-situ* measurements.

The use of the *in-situ* referencing of the impulsive excitation was demonstrated in the CARS imaging thermometry performed across the flame front of a laminar, premixed methane/air flame (Φ=0.95). In the scope of the present work, the location of the flame front was defined as the measurement point yielding the closest temperature to 1192 K, this value corresponding to the inflection point of the temperature profile across the reaction layer of the measured flame, as computed by the CHEM1D code [48]. The comparison of the temperature evaluations, obtained by applying the two referencing methods on 900 single-shot CARS spectra acquired in the flame, is discussed in the following.

In Fig. 5, the probability density functions (PDFs) of the temperature measurements are provided as a mean of comparison for the *ex-situ* and *in-situ* referencing techniques. The same resonant spectra, acquired in a 900 frames

sample, were thus referenced by: 1. the time-averaged non-resonant spectrum acquired in room-temperature argon (*ex-situ*), and 2. the single-shot non-resonant spectra acquired in the second detection channel, simultaneously to the resonant one (*in-situ*).

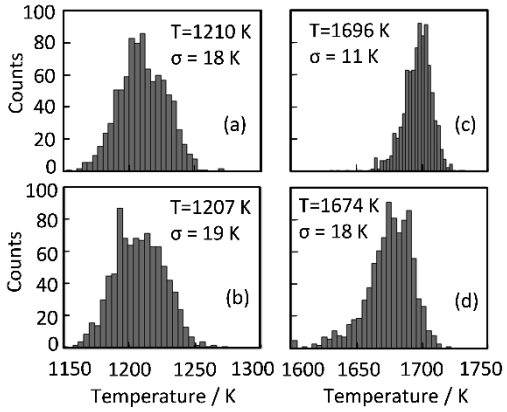

Fig. 5. Probability density functions of the 900 single-shot CARS-evaluated temperatures in the oxidation region of a laminar premixed methane/air flame. (a-b) Comparison for the measurements performed at ~65 μm from the flame-front. The *ex-situ* CARS measurement resulted in an average temperature of 1210 K, with standard deviation of 18 K (~1.5%); the *in-situ* referencing provided an average temperature of 1207 K, with standard deviation of 19 K (~1.6%). (c-d) Comparison of the temperature assessment provided by *ex-situ* and *in-situ* referencing of the resonant CARS spectra acquired at ~455 μm from the flame-front. The *ex-situ* referencing resulted in an average temperature of 1696 K, with standard deviation 11 K (~0.7%); the *in-situ* provided an average temperature of 1674 K with standard deviation 18 K (~1.1%).

The *ex-situ* and *in-situ* referencing of the resonant spectra yielded in the temperature measurements at ~455 μm from the flame-front, respectively: 1. an average temperature of 1696 K, with standard deviation 11 K (~0.7%); 2. an average temperature of 1674 K with standard deviation 18 K (~1.1%). The *ex-situ* referencing of the resonant CARS spectra results in a consistent bias towards higher temperatures, as compared to the results of the *in-situ* referencing: the systematic bias being quantified in 22 K (~1.3%) at this flame location. This behavior is in good agreement with the aforementioned discrepancy in the available excitation bandwidth as mapped by NR spectra acquired *in-situ* and *ex-situ*: the lower density of the hot product gases is expected to have a lesser GVD on the ultrashort pump/Stokes pulses, thus resulting in a broader effective bandwidth. The effect of the temperature of the gaseous medium on the GVD of the fs pump/Stokes, is even more evident when comparing the CARS measurements provided by *ex-situ* and *in-situ* referencing, at lower temperatures. Indeed, at a distance of ~65 μm from the flame-

front the two referencing techniques yielded the following results: 1. an average temperature of 1210 K (*in-situ*) and 2. an average temperature of 1210 K (*ex-situ*). The evident decrease in the systematic bias of the ex-situ referenced CARS thermometry is well understood as a lesser impact the GVD on the pump/Stokes pulse.

It is nonetheless important to note that the CARS-evaluated temperatures seem to be significantly lower than as predicted by the numerical model of the laminar, premixed methane/air flame-front: the expected temperature is indeed ~1870 K. This higher temperature value was moreover confirmed by performing CARS measurements at longer probe pulse delay (~27 ps), i.e. where the probe pulse is not temporally overlapped to the pump/Stokes pulse, and the self-referencing technique can thus not be employed. As a matter of fact, these measurement provide an average temperature of ~1840 K (~1.6%). The reported discrepancy between the temperature measurements performed at long and short (i.e. within the temporal overlap of the pump/Stokes and probe pulses) pump-probe delay was consistently observed in different measurement locations within the flame-front and for different values of the delay itself. This behavior seems to indicate the presence of a source of uncertainty in the evaluation of the temperature through the resonant CARS spectra generated at short pump-probe delays, which our theoretical model fails to take into account. Nevertheless, this uncertainty is not inherent to the *in-situ* referencing of the impulsive excitation, as it was also clearly observed in the temperature measurements provided by the *ex-situ* referencing by room-temperature argon.

As far as the relative standard deviation of the temperature measurements is concerned, the self-referencing shows a slightly worse precision as compared to the *ex-situ* referencing. This is attributed to the reduced SNB ratio available in the single-shot detection of the non-resonant signal in the self-referencing approach. Seemingly, this effect was more pronounced than any shot-to-shot variation in the effective excitation bandwidth, that the *in-situ* referencing could have accounted for. Nonetheless, the use of the self-referencing technique here described could provide a substantial improvement in the precision of CARS thermometric measurements in a number of applications of practical interest. The variance in the bandwidth of the fs pump/Stokes pulse is expected to play a major role e.g. in high-pressure applications, highly turbulent environments, large-scale combustors and all those application employing ultra-broadband laser sources.

Conclusions

The simultaneous, *in-situ* referencing of the resonant Raman spectra was achieved by the concurrent, spatially divided detection of the resonant and non-resonant CARS signals in two distinct por- tions of the same detector frame. The non-resonant CARS signal detected in Channel 2 was thus em- ployed as a spectral reference to the resonant CARS signal detected in Channel 1. Furthermore, we successfully demonstrated the application of this technique to the spatially correlated data provided by a single-shot one-dimensional CARS imaging system. Moreover, we have investigated the impact of the spectral referencing on CARS flame thermometry. A consistent bias of the *ex- situ* referencing towards higher temperatures was reported. This is understood in terms of the effect of the GVD change in the less dense product gases, as compared to the room-temperature argon employed to measure the *ex-situ* non-resonant spectrum. Nonetheless, the mean temperatures provided by both referencing methods were lower than predicted by the numerical evaluation of the measured flame front. This temperature bias was further more confir med by additional CARS mea- surements performed at longer pump-probe delays, where no *in-situ* referencing is possible. In terms of relative standard deviation, the CARS-evaluated temperature obtained by applying the *in-situ* ref- erencing was slightly worse than the *ex-situ* case. Nevertheless, the self-referencing technique here proposed is foreseen to improve the thermomet- ric precision in more challenging measurement conditions.

Acknowledgements

We gratefully acknowledge the financial support provided by the Netherlands Organization for Scientific Research (NWO), obtained through a Vidi grant in the Applied and Engineering Sciences domain (AES) (15690).

References

[1] K. Kohse-Höinghaus, R. S. Barlow, M. Aldén, E. Wolfrum, Combustion at the focus: laser diagnostics and control, Proc. Combust. Inst. 30 (2005) 89-123.

[2] A. C. Eckbreth, Laser Diagnostics for Combustion Temperature and Species, 2nd ed., (Gordon and Breach: Amsterdam, 1996).

[3] S. Druet, J. P. Taran, CARS spectroscopy, Prog. Quant. Electr., 7 (1981), pp. 1-72

[4] D. I. Greenhalgh, Quantitative CARS spectroscopy, Adv Spectrosc, 15 (1988), pp. 193-251

[5] S. Roy, J. R. Gord, A. K. Patnaik, Recent advances in coherent anti-Stokes Raman scattering spectroscopy: Fundamental developments and applications in reacting flows, Prog. Energ. Combust 36 (2010) 280.

[6] T. Seeger, A. Leipertz, Experimental comparison of single-shot broadband vibrational and dual-broadband pure rotational coherent anti-Stokes Raman scattering in hot air. Appl. Opt. 35 (1996) 2665-2671

[7] A. Bohlin, E. Nordström, H. Carlsson, X.-S. Bai, P.-E. Bengtsson, Pure rotational CARS measurements of temperature and relative O_2-concentration in a low swirl turbulent premixed flame, Proc. Combust. Inst. 34 (2013) 3629.

[8] R. E. Palmer, Sandia CARSFT code, Report No. SAND89-8206, Sandia National Laboratories, Livermore, CA, USA, 1989.

[9] L. Martinsson, P.-E. Bengtsson, M. Aldén, S. Kröll, J. Bonamy, A test of different rotational Raman linewidth models: Accuracy of rotational coherent anti-Stokes Raman scattering thermometry in nitrogen from 295 to 1850 K, J. Chem. Phys. 1993, 99(4), 2466.

[10] M. Marrocco, Herman–Wallis factor to improve thermometric accuracy of vibrational coherent anti-Stokes Raman spectra of H_2 , Proc. Combust. Inst. 32 (2009) 863-870.

[11] S. Kröll, M. Aldén, T. Berglind, and R. J. Hall, Noise characteristics of single shot broadband Raman-resonant CARS with single- and multimode lasers, Appl. Opt. 26 (1987) 1068-1073.

[12] J. P. Kuehner, M. A. Woodmansee, R. P. Lucht, J. C. Dutton, High-resolution broadband N_2 coherent anti-Stokes Raman spectroscopy: comparison of measurements for conventional and modeless broadband dye lasers, Appl. Opt. 42 (2003) 6757-6767.

[13] M. Woyde and W. Stricker, The application of CARS for temperature measurements in high pressure combustion systems, Appl. Phys. B 50 (1990) 519-525.

[14] T. Lundeen, S. Y. Hou, J. W. Nibler, Non-resonant 3rd order susceptibility for various gases, J. Chem. Phys. 79 (1983) 6301-6305.

[15] R. L. Farrow, R. P. Lucht, L. A. Rahn, Measurements of the nonresonant 3rd order susceptibilities of gases using coherent anti-Stokes Raman spectroscopy, J. Opt. Soc. Am. B., 4 (1987) 1241-1246.

[16] F. Grisch, P. Bouchardy, W. Clauss, CARS thermometry in high pressure rocket combustors, AEROSP SCI TECHNOL, 7 (2003) 317–330.

[17] S. A. Tedder, J. L. Wheeler, A. D. Cutler, P. M. Danehy, Width-increased dual-pump enhanced coherent anti-Stokes Raman spectroscopy, Appl. Opt. 49 (2010) 1305-1313.

[18] W.F. Murphy, Rayleigh Depolarisation Ratio and Rotational Raman-Spectrum of Water-Vapour and Polarizability Components for Water Molecule, J. Chem. Phys. 67 (1977) 5877-5882.

[19] C. C. Hayden, D. W. Chandler, Femtosecond time-resolved studies of coherent vibrational Raman scattering in large gas-phase molecules, J. Chem. Phys. 103 (1995) 10465−10472.

[20] T. Lang, M. Motzkus, Single-shot femtosecond coherent anti-Stokes Raman-scattering thermometry, J. Opt. Soc. Am. B. 19 (2002) 340.

[21] R. P. Lucht, S. Roy, T. R. Meyer, J. R. Gord, Femtosecond coherent anti-Stokes Raman scattering measurement of gas temperatures from frequency-spread dephasing of the Raman coherence, Appl. Phys. Lett. 89 (2006) 251112

[22] W. D. Kulatilaka, P.S. Hsu, H. U. Stauffer, J. R. Gord, S. Roy, Direct measurements of rotationally resolved H_2 Q-branch Raman coherence lifetimes using time-resolved picosecond coherent anti-Stokes Raman scattering, Appl. Phys. Lett. 97 (2010) 081112.

[23] D. Pestov, R. K. Murawski, G. O. Ariunbold, X. Wang, M. C. Zhi, A. V. Sokolov, V. A. Sautenkov, Y. V. Rostovtsev, A. Dogariu, Y. Huang, M. O. Scully, Optimizing the laser-pulse configuration for coherent Raman spectroscopy, Science 316 (2007) 265–268.

[24] T. Seeger, J. Kiefer, A. Leipertz, B. D. Patterson, C. J. Kliewer, T. B. Settersten, Picosecond time-resolved pure-rotational coherent anti-Stokes Raman spectroscopy for N_2 thermometry, Opt. Lett. 34 (2009) 3755-3757.

[25] D. R. Richardson, H. U. Stauffer, S. Roy, J. R. Gord, Comparison of chirped-probe-pulse and hybrid femtosecond/picosecond coherent anti-Stokes Raman scattering for combustion thermometry, Appl. Opt. 56 (2017) 37–49.

[26] S. P. Kearney, Hybrid fs/ps rotational CARS temperature and oxygen measurements in the product gases of canonical flat flames, Combust. Flame, 162 (2015) 1748-1758.

[27] A. Bohlin, C. J. Kliewer, Direct coherent Raman temperature imaging and wideband chemical detection in a hydrocarbon flat flame, J. Phys. Chem. Lett. 6 (2015) 643-649.

[28] R.S. Barlow, Laser diagnostics and their interplay with computations to understand turbulent combustion, Proc. Combust. Inst. 31 (2007) 49-75.

[29] G. Magnotti, A. D. Cutler, P. M. Danehy, Beam shaping for CARS measurements in turbulent environments," Appl. Opt. 51 (2012) 4730-4741.

[30] E. H. van Veen, D. Roekaerts, Thermometry for turbulent flames by coherent anti-Stokes Raman spectroscopy with simultaneous referencing to the modeless excitation profile, Appl. Opt. 44 (2005) 6995-7004.

[31] A. C. Eckbreth, T. J. Anderson, Simultaneous Rotational Coherent Anti-Stokes Raman-Spectroscopy and Coherent Stokes Raman-Spectroscopy with Arbitrary Pump Stokes Spectral Separation, Opt. Lett. 11 (1986) 496−498.

[32] M. Aldén, P.-E. Bengtsson, H. Edner, Rotational CARS generation through a multiple four-color interaction, Appl. Opt. 25 (1986) 4493−4500.

[33] B. D. Prince, A. Chakraborty, B. M. Prince, H. U. Stauffer, Development of simultaneous frequency-and time-resolved coherent anti-Stokes Raman scattering for ultrafast detection of molecular Raman spectra, J. Chem. Phys. 125 (2006) 044502.

[34] J. D. Miller, S. Roy, M. N. Slipchenko, J. R. Gord, T. R. Meyer, Single-shot gas-phase thermometry using pure-rotational hybrid femtosecond/picosecond coherent anti-Stokes Raman scattering, Opt. Express, 19 (2011) 15627-15640.

[35] A. Bohlin, M. Mann, B. D. Patterson, A. Dreizler, C. J. Kliewer, Development of two-beam femtosecond/picosecond one-dimensional rotational coherent anti-Stokes Raman spectroscopy: time-resolved probing of flame wall interactions, Proc. Combust. Inst. 35 (2015) 3723–3730.

[36] M. Scherman, M. Nafa, T. Schmid, A. Godard, A. Bresson, B. Attal-Tretout, P. Joubert, Rovibrational hybrid fs/ps CARS using a volume Bragg grating for N_2 thermometry, Opt. Lett., 41 (2016) 488-491.

[37] C. B. Yang, D. Escofet-Martin, D. Dunn-Rankin, Y. C. Chien, X. Yu, S. Mukamel, Hybrid femtosecond/picosecond pure-rotational coherent anti-Stokes Raman scattering with chirped probe pulses, J. Raman Spectrosc. 48 (2017) 1881.

[38] Y. Ran, M. Junghanns, A. Boden, S. Nolte, A. Tünnermann, R. Ackermann, Temperature and gas concentration measurements with vibrational ultra-broadband two-beam femtosecond/picosecond coherent anti-Stokes Raman scattering and spontaneous Raman scattering, J. Raman Spectrosc. 50, 9 (2019) 1268.

[39] J. E. Retter, G. S. Elliott, On the possibility of simultaneous temperature, species, and electric field measurements by coupled hybrid fs/ps CARS and EFISHG, Appl. Opt. 58 (2019) 2557-2566.

[40] N. Owschimikow, B. Schmidt, N. Schwentner, Laser-induced alignment and anti-alignment of rotationally excited molecules, Phys. Chem. Chem. Phys., 13 (2011) 8671–8680.

[41] F. Vestin, M. Afzelius, P.-E. Bengtsson, Development of rotational CARS for combustion diagnostics using a polarization approach, Proc Combust Inst, 31 (2007) 833-840.

[42] A. Bohlin, B.D. Patterson, C.J. Kliewer, Communication: Simplified two-beam rotational CARS signal generation demonstrated in 1D, J. Chem. Phys. 138 (2013) 081102.

[43] L. Castellanos , F. Mazza , D. Kliukin , A. Bohlin , Pure-rotational 1D-CARS spatiotemporal thermometry with a single regenerative amplifier system. Opt. Lett. 45 (2020) 4662–4665 .

[44] S. P. Kearney, D. J. Scoglietti, Hybrid femtosecond/picosecond rotational coherent anti-Stokes Raman scattering at flame temperatures using a second-harmonic bandwidth-compressed probe, Opt. Lett. 38 (2013) 833-835.

[45] F. Raoult, A. C. L. Boscheron, D. Husson, C. Sauteret, A. Modena, V. Malka, F. Dorchies, A. Migus, Efficient generation of narrow-bandwidth picosecond pulses by frequency doubling of femtosecond chirped pulses, Opt. Lett. 23 (1998) 1117-1119.

[46] A. Bohlin, C.J. Kliewer, Single-shot hyperspectral coherent Raman planar imaging in the range 0–4200 cm^{-1}, Appl. Phys. Lett. 105 (2014) 161111.

[47] P. J. Wrzesinski, D. Pestov, V. V. Lozovoy, J. R. Gord, R. J. Sukesh, Group-velocity-dispersion measurements of atmospheric and combustion-related gases using an ultrabroadband-laser source, Opt. Express, 19 (2011) 5163-5171.

[48] J. A. van Oijen, L. P. H. de Goey, Modelling of premixed laminar flames using flamelet-generated manifolds, Combust. Sci. and Tech. 161 (2000) 113-137.

Figure Captions

Figure 1. The polarisation sensitive wide-field coherent imaging spectrometer used for spatially divided detection of resonant - and non-resonant femtosecond/picosecond one-dimensional (1D) coherent anti-Stokes Raman spectroscopy (CARS) signals. Astigmatic convergence of the sheet forming optics is used to enhance the irradiance of the probe-beam at the measurement location. The indexes v (vertically) and h (horizontally) express the alignment symmetry axis of the cylindrical lenses. Two separate detection channels for P- and S-polarized light (orientation determined with respect to the transmission grating), respectively are relay-imaged with ~1:1 magnification from the signal generation plane to the position of the detector.

Figure 2. Single-shot detection of concurrent resonant and non-resonant pure-rotational femtosecond/picosecond 1D-CARS signals acquired *in-situ* across the flame-front of a laminar premixed methane/air flame (Φ=0.95). The two CARS signal components are generated with a relative probe-pulse delay of ~3 ps. The label "Channel 1" indicates portion of the detector frame employed for the acquisition of the resonant CARS signal, which is dominated by the characteristic spectral signature of N_2. "Channel 2" indicates the detection channel for the broadband non-resonant CARS signal (due to four-wave-mixing), which is scattered from all the species present probed volume.

Figure 3. . Single-shot, femtosecond/picosecond resonant CARS spectrum, generated as short pump-probe pulse delay (~3ps) and acquired at ~450 μm from the flame-front of a premixed methane/air flame (Φ=0.95). The resonant spectrum, acquired in first detection channel, was back-ground subtracted and referenced to the non-resonant CARS spectrum acquired simultaneously in the second detection channel. In order to determine the corresponding temperature, the resulting spectrum was compared to a library of synthetic spectra, computed by means of a time-resolved CARS code. The resulting temperature in the measurement location was thus assessed in 1630 K. The performance of the spectral fitting can be evaluated by the residuals of the theoretical and experimental spectra, which are presented in the figure, with an offset of -0.2 for clarity purposes.

Figure 4. (Top) Comparison of the average non-resonant spectra acquired in room-temperature argon (*ex-situ*) and at ~455 μm from the flame-front in a laminar, premixed methane/air flame (Φ=0.95). (Bottom) The relative standard deviation as obtained from the 900 instantaneous recordings, respectively.

Figure 5. Probability density functions of the 900 single-shot CARS-evaluated temperatures in the oxidation region of a laminar premixed methane/air flame. (a-b) Comparison for the measurements performed at ~65 μm from the flame-front. The *ex-situ* CARS measurement resulted in an average temperature of 1210 K, with standard deviation of 18 K (~1.5%); the *in-situ* referencing provided an average temperature of 1207 K, with standard deviation of 19

K (~1.6%). (c-d) Comparison of the temperature assessment provided by *ex-situ* and *in-situ* referencing of the resonant CARS spectra acquired at ~455 μm from the flame-front. The *ex-situ* referencing resulted in an average temperature of 1696 K, with standard deviation 11 K (~0.7%); the *in-situ* provided an average temperature of 1674 K with standard deviation 18 K (~1.1%).